Article

Controllable Porosity of Monodispersed Tin Oxide Nanospheres via an Additive-Free Chemical Route

S. Y. Ho, A. S. W. Wong, and G. W. Ho

Cryst. Growth Des., **2009**, 9 (2), 732-736• DOI: 10.1021/cg8001256 • Publication Date (Web): 09 December 2008

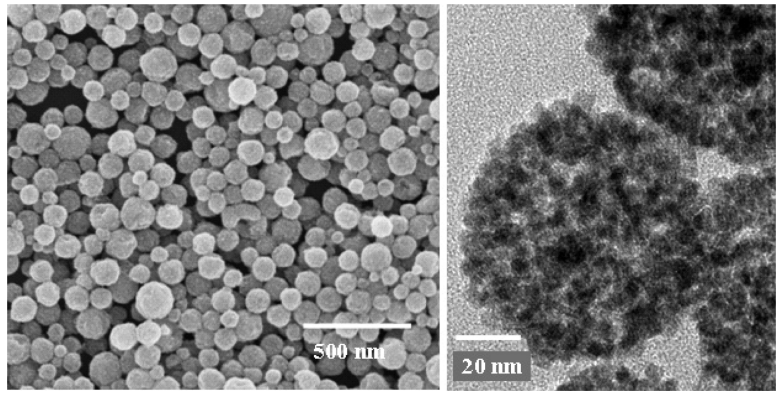

CRYSTAL GROWTH & DESIGN
2009
VOL. 9, NO. 2
732–736

Controllable Porosity of Monodispersed Tin Oxide Nanospheres via an Additive-Free Chemical Route

S. Y. Ho,[†] A. S. W. Wong,[‡] and G. W. Ho*[,†,§]

*Department of Electrical and Computer Engineering, National University of Singapore, 4 Engineering Drive, Singapore 117576, Engineering Science Programme, National University of Singapore, 9 Engineering Drive 1, Singapore 117576, and Institute of Materials Research and Engineering, A*STAR (Agency for Science Technology and Research), 3 Research Link, Singapore 117602*

Received February 2, 2008; Revised Manuscript Received October 13, 2008

ABSTRACT: Tin dioxide (SnO_2) nanospheres with various degrees porosity have been successfully synthesized via a facile, easily scalable, and tunable hydrothermal process. The employed method requires no physical templates or environmentally unfriendly additives. Elimination of additives was favorably found to increase the specific surface area and reduce the organic contamination issue in the end product. Investigation of the controllable synthesis and growth mechanism provides valuable insights into studies of the fundamental properties of mesoporous tin oxides nanospheres. The as-synthesized mesoporous SnO_2 nanospheres are composed of numerous small nanocrystallites ~5−10 nm and possess good size uniformity and large specific surface areas, making them excellent candidates for use in industrial applications such as gas sensors, catalysts, and biomedical drug therapy.

Introduction

As an n-type semiconductor with a wide band gap ($E_g = 3.6$ eV), tin dioxide SnO_2 has generated considerable research effort due to its applicability in a myriad of fields such as gas sensors, optoelectronic devices, catalysts, and lithium rechargeable batteries.[1−4] In addition, there has been growing interest in the fabrication of hollow or porous inorganic nanostructures for use as drug-delivery carriers,[5] capsules for controlled release of cosmetics, catalysts, and gas sensors.[6] The large specific surface area of these porous nanostructures makes them very reactive materials since a high proportion of atoms is located at the surface of the nanocrystals.[7] It was reported that hollow SnO_2 nanospheres exhibited enhanced room-temperature gas sensitivity as compared to SnO_2 nanoparticles of the same size.[8] The superior sensing performance can be attributed to the higher surface area of hollow SnO_2 nanospheres, which provides more sites for surface adsorption and desorption of the gas molecules.

Hollow or porous nanostructures have typically been synthesized with the assistance of hard templates like sacrificial polymeric core supports[9] or soft templates like micelles.[10] However, removal of hard templates requires complex synthetic procedures and high costs which limit their use in large-scale productions,[11] while soft templating routes suffer from instability problems which require introduction of complex surfactant systems.[12] Large-scale self-assembly of nanostructured building components has attracted significant interest. Various self-assembly processes based on different driving forces exist, among which the oriented attachment proved to be an effective mechanism for synthesizing mesoporous structures. It is also noted that additive-free synthesis of nanostructures and self-assembling them into well-defined structures remains a huge challenge. Herein we report a successful facile self-assembly, template, and additive-free synthesis of mesoporous SnO_2 nanostructures via an oriented attachment growth mechanism. The SnO_2 nanostructures obtained possess high specific surface areas, and their dimensions and structural morphologies can be well controlled via changes in reaction conditions.

Experimental Section

Mesoporous nanospheres were synthesized through a simple hydrothermal method using potassium stannate trihydrate ($K_2SnO_3 \cdot 3H_2O$, Aldrich 99.9%) as a precursor in an ethanol−deionized water mixed solvent.[13] In a typical experiment, 5 mmol (mM) of $K_2SnO_3 \cdot 3H_2O$ was dissolved in 30 mL of an ethanol−deionized water mixture (equal volumes of ethanol and water). After stirring for 5 min, a homogeneous solution was obtained and 0.1 M urea was added to the mixture before transferring to a 40 mL Teflon-lined stainless steel autoclave. The autoclave was maintained at 150 °C for 24 h and then cooled naturally to room temperature. The resulting white precipitate was centrifuged and thoroughly washed with ethanol before drying in air at 40 °C. The parameters affecting the morphology and porosity of the synthesized SnO_2 nanostructures were investigated by varying various experimental conditions.

Scanning electron microscopy (SEM) observations were carried out on a FESEM JSM-6700F operating at 10 kV. Transmission electron microscopy (TEM) characterisations were conducted using a JEOL-2100 TEM with an accelerating voltage of 200 kV. X-ray diffraction (XRD) experiments were performed on a Bruker GADDS XRD using monochromatized Cu Kα ($\lambda = 0.154$ nm) radiation under 40 kV and 40 mA. X-ray photoelectron spectroscopy (XPS) experiments were done using a VG ESCALAB MK2 equipped with an Mg Kα X-ray source operating at 300 W. Fourier transform infrared (FTIR) spectroscopy was performed on a Bio-Rad FTIR FTS 135 spectrometer. Brunauer−Emmett−Teller (BET) measurements were conducted using a BET Surface Area and Pore Analyzer Autosorb (NOVA 3000) with N_2 as the adsorbate at liquid nitrogen temperature.

Results and Discussion

The morphology of the SnO_2 nanostructures produced under reference conditions is shown in Figure 1a and 1b. Well-dispersed nanospheres of diameters between 50 and 150 nm were obtained. The phase and purity of the sample were determined by XRD. Figure 2a illustrates the typical diffraction pattern, and all the peaks can be well indexed to a tetragonal rutile SnO_2 structure (JCPDS card No. 41-1445, $a_o = 4.738$ Å, $c_o = 3.187$ Å). No characteristic peaks were observed for other impurities. To further characterize the product, XPS analysis was conducted to investigate the surface compositions and

* To whom correspondence should be addressed. E-mail: elehgw@nus.edu.sg.
[†] Department of Electrical and Computer Engineering, National University of Singapore.
[‡] A*STAR.
[§] Engineering Science Programme, National University of Singapore.

10.1021/cg8001256 CCC: $40.75
Published on Web 12/09/2008

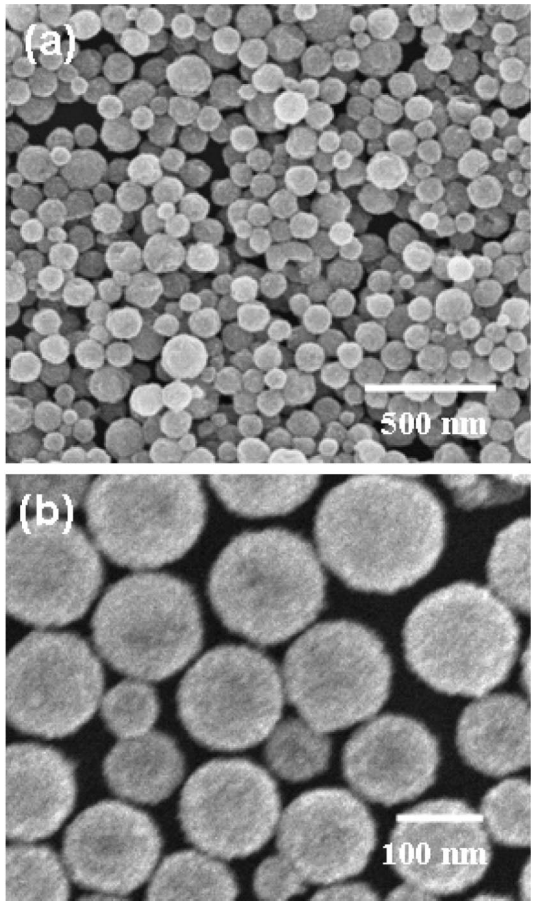

Figure 1. SEM images of the as-synthesized SnO_2 nanospheres at (a) low and (b) high magnification.

chemical state of the as-prepared products. Specimen charging was accounted for by referencing C1s to 284.5 eV. Figure 2b shows that the Sn3d spectrum of the sample, which appears as a spin−orbit doublet at ∼486.8 ($3d_{5/2}$) and ∼495.3 eV ($3d_{3/2}$), is in good agreement with the values given in the literature.[14] The O1s binding energy of 530.7 eV (Figure 2c) indicates that oxygen atoms exist as O^{2-} species, while the binding energy of 531.8 eV is attributed to OH^- hydroxyl groups or chemisorbed molecular oxygen (O_2^-) in the products.[8]

Both the XRD and XPS results verify that the as-synthesized products are indeed SnO_2. TEM was used to elucidate the interior structure of the nanospheres. Figure 3a shows that the nanospheres have rough surfaces and are rather solid in texture. The high-resolution image (Figure 3b) reveals that each nanosphere is made up of numerous primary nanocrystallites with a diameter of ∼5−10 nm. Clear lattice fringes are observed, and *d* spacings are measured to be 0.26 and 0.33 nm, which can be indexed to the SnO_2 (101) and (110) crystal planes, respectively (Figure 3c).

We systematically investigated various reaction parameters to tune the morphology and porosity of the SnO_2 nanostructures. It was found that the reaction time played an important role in hollowing out the interior of the nanospheres. Using the nanospheres obtained at 5 mM precursor concentration and keeping the temperature constant at 150 °C the TEM images in Figure 4a−c clearly illustrate the changes in the porosity of the nanostructures with the increase of reaction times from 6, 12, and 48 h respectively. The sizes of the nanospheres remain relatively unchanged, but with prolonged hydrothermal treatment the interior of the nanospheres is subjected to a dissolution

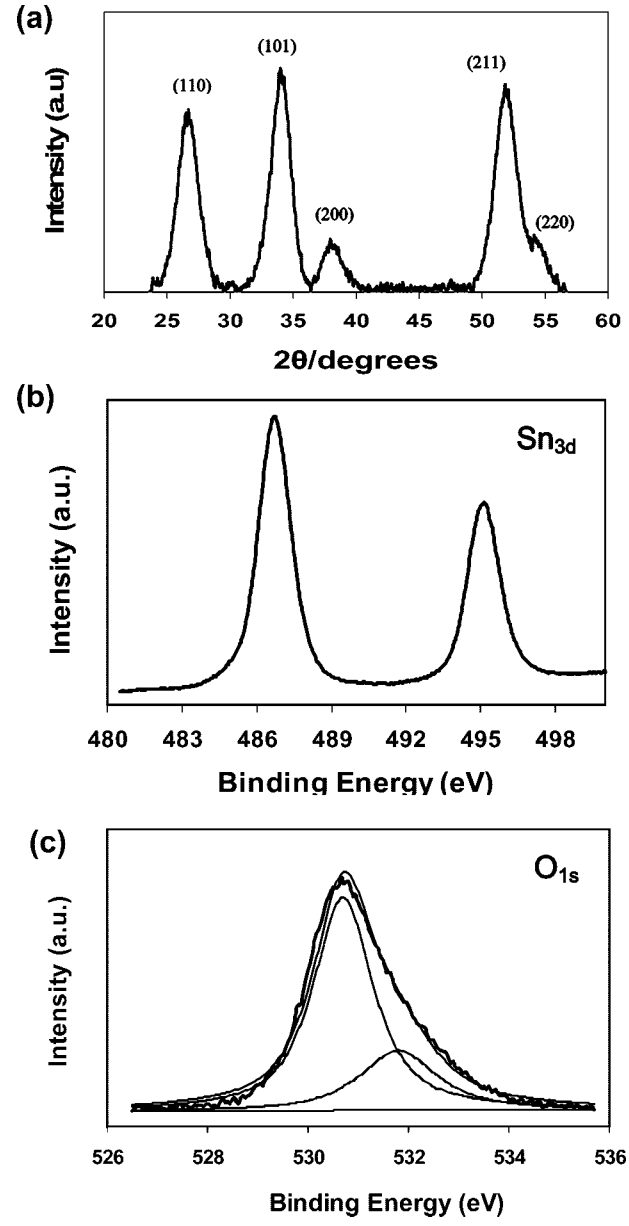

Figure 2. (a) XRD and XPS spectra of (b) Sn3d and (c) O1s of the SnO_2 nanospheres.

process, leading to spheres of greater porosity. Next, temperature-dependent experiments were carried out at 150, 200, and 225 °C grown for 12 h and keeping other experimental parameters constant. From the TEM images in Figure 4d−f it is evident that the reaction temperature is also a key factor affecting the degree of porosity. At higher temperatures dissolution of nanocrystallites increased and formed a more porous structure. A possible explanation for the greater porosity is that higher reaction temperatures may have facilitated dissolution of nanocrystallites. As porosity is closely linked to specific surface area,[8,15] the increased porosity of the nanospheres can be further confirmed by BET studies (discussed later), which measure the specific surface area of the samples.

Figure 4g illustrates the possible formation process of the mesoporous SnO_2 spheres based on electron microscopy analyses. During the initial stage of the synthesis hydrolysis of potassium stannate trihydrate leads to formation of numerous nanocrystallites. These primary nanocrystallites aggregate to form nanospheres, driven by the mechanism of overall surface

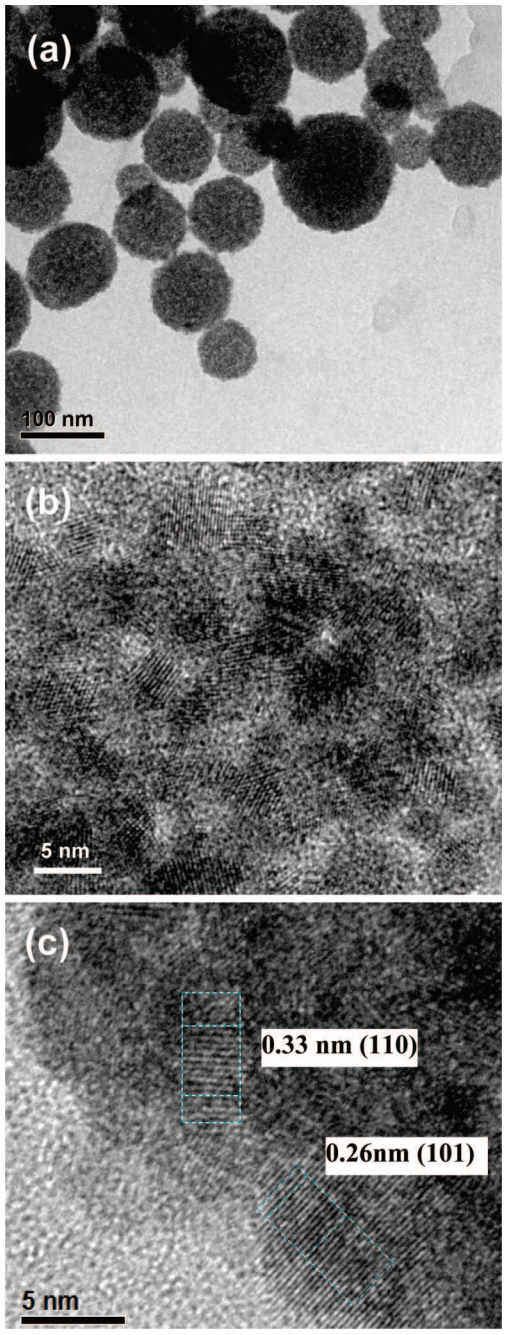

Figure 3. TEM images of SnO_2 nanostructures dispersed on carbon grid. (a) Bright-field, low-magnification images of mesoporous SnO_2 nanospheres. (b) HRTEM image of nanocrystallites inside each nanosphere (c) Measured interplanar spacings that can be indexed to the SnO_2 (101) and (110) crystal planes.

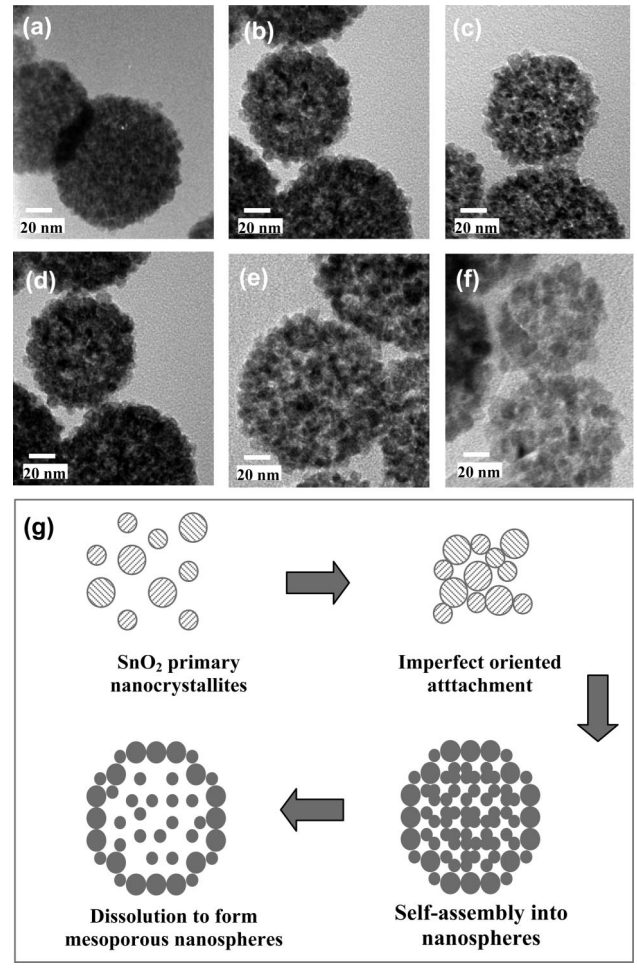

Figure 4. TEM images of nanospheres grown at different reaction times of (a) 6, (b) 12, and (c) 48 h at 150 °C. TEM images of nanospheres grown at different reaction temperatures of (d) 150, (e) 200, and (f) 225 °C for 12 h. (g) Schematic diagram of the growth mechanism of the SnO_2 mesoporous spheres.

energy reduction. Formation of nanospheres by aggregation of nanocrystallites can be closely referred to the imperfect oriented attachment mechanism.[16] This mechanism is based on self-assembly of primary nanocrystallites followed by spontaneous lattice fusion of the adjacent crystallographic planes in an ideal liquid environment medium. These nanocrystallites possess high surface energies and easily aggregate at an early stage of the hydrothermal growth process. Since there is no specific crystal plane orientation anisotropic crystal growth in unidirection is not observed. The nanocrystallites are randomly oriented but on a whole self-assembled to form spherical nanospheres. Compared to those in the outer surfaces, nanocrystallites in the inner regions have larger surface energies as they can be visualized as being part of a smaller sphere with higher curvature.[17] As a result of larger surface energies the inner nanocrystallites have a stronger tendency to dissolve and a hollowing out effect is achieved as reaction time or temperature increases. Another postulation has also been made on the hollowing effect of the interior part of the nanospheres. It has been reported that the primary nanocrystallites on the outer surfaces are more well crystallized than the interior part of the nanospheres since crystallization of the outer surfaces is highly promoted by the copious surrounding solvent during hydrothermal treatment.[13] This leads to a highly dissolution-resistance outer region of the nanospheres. As the reaction temperature or time is increased we observed that the resulting product has insignificantly increased in diameter. It is believed that dissolution of nanocrystallites may have redeposited on existing small nanospheres via an Ostwald ripening process or forms new nanospheres since it is noted that a high yield (>95%) of the end product is recovered after the synthesis process.[13]

The following experiments were carried out to validate our proposition that addition of additives (urea) can unfavorably decrease the specific surface area and introduce organic contaminant in the end product. To do so, samples were prepared without (Figure 5a−c) and with (Figure 5d−f) addition of 0.1 M urea at 5, 10, and 20 mM $K_2SnO_3 \cdot 3H_2O$. For the case of synthesis without urea, at a low precursor concentration of 5

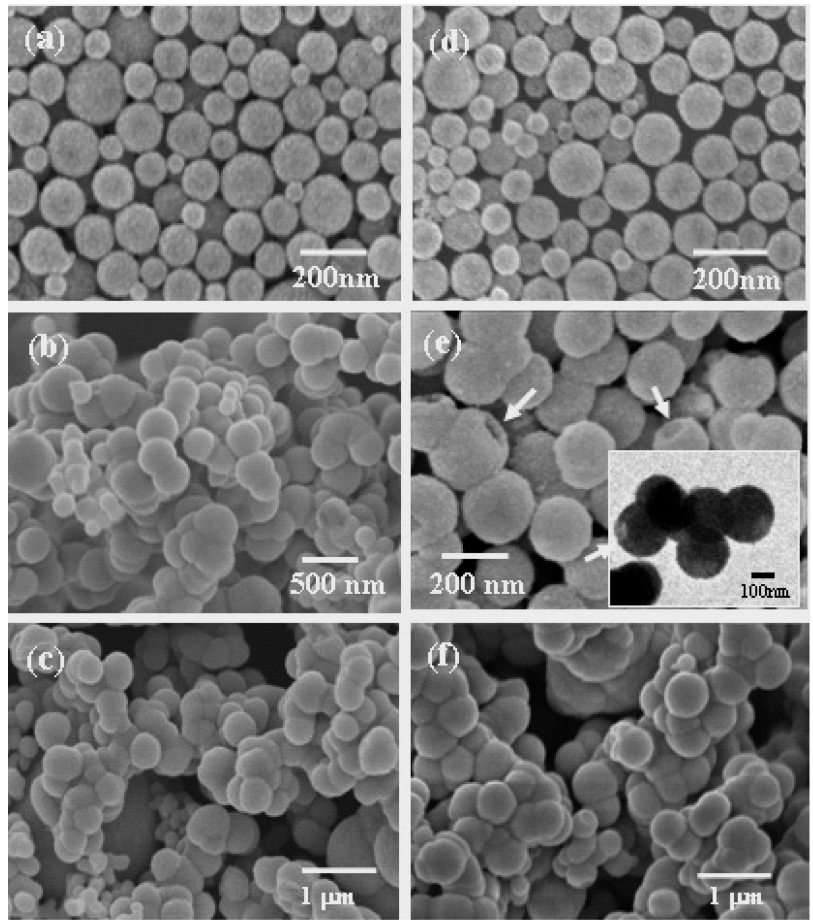

Figure 5. SEM images of SnO_2 nanostructures prepared without urea at three different precursor concentrations of (a) 5, (b) 10, and (c) 20 mM as well as with urea at (d) 5, (e) 10, and (f) 20 mM precursor concentrations.

mM the absence of urea yielded monodispersed nanospheres. As the precursor concentration was increased to 10−20 mM, severe agglomeration occurred as the nanostructure loses its spherical morphology and forms irregular structures. For the case of the synthesis with urea, the nanospheres synthesized at 5 mM show insignificant morphology changes or size distribution improvements as compared with those synthesized without the aid of urea additives. The diameters of the nanospheres are still in the range of 50−200 nm. On the other hand, at a higher precursor concentration of 10 mM, with the use of urea, the nanospheres are observed to retain most of their morphology and dispersivity characteristics except that the diameters have increased to 100−400 nm. Some bowl-like and partial agglomerated structures were observed from both the SEM and TEM images (Figure 5e). From the TEM observation (Figure 5e, inset), the nanospheres obtained at higher precursor concentration appeared to be less porous. High-magnification TEM images (not shown here) show that the nanospheres synthesized at higher precursor concentration are made up of densely packed nanocrystallites. With further increases of the precursor concentration to 20 mM, severe agglomeration sets in even with addition of urea (Figure 5f). The driving force behind agglomeration of nanostructures is the reduction of the overall surface energy of the system. It is imperative to prevent agglomeration as the process is usually irreversible. It has previously been reported that urea aids in stabilization of the primary nanocrystals by adsorbing on them and hence reducing the chances of agglomeration up to a critical precursor concentration. The hydrogen-bond interactions between the adsorbed urea molecules also help to assemble the primary nanocrystals into spherical aggregates.[18] The total interaction between any two particles in a suspension is a combination of van der Waals attraction and electrostatic repulsion. The electrostatic repulsion potential is a function of precursor ion concentration.[19] It is postulated that urea was not required to obtain well-dispersed nanospheres at low precursor concentrations (dilute system) since the electric repulsion potential dominates over the van der Waals attraction between adjacent nanospheres.

It is important to note that nanospheres synthesized at a low precursor concentration regime is of interest since the obtained nanostructures are higher in porosity as well as smaller in diameter. Effectively, urea is eliminated from our synthesis procedures. FTIR spectra (Figure 6) of the nanospheres prepared with and without urea provide clear evidence that urea molecules remain incorporated in the SnO_2 nanospheres. The bands at 3000, 1650, and 1435 cm^{-1} can be assigned to the N−H and C═O stretching modes and the N−C−N antisymmetric stretching vibration, respectively.[17] The intense bands at lower frequencies of ∼700 cm^{-1} on each spectrum are typical of Sn−O−Sn symmetric and asymmetric stretches,[20] while the band around 3450 cm^{-1} can be attributed to the O−H stretch of adsorbed water. The band at 2300 cm^{-1} corresponds to residual CO_2 in the atmosphere.[21] Thus, it is evident that urea molecules are present in the SnO_2 nanospheres. Elimination of urea from the synthesis process is very important since it removes any organic contaminant as well as dismisses the need for subsequent high-temperature annealing to remove the adsorbed urea components.

Figure 7 shows the nitrogen adsorption−desorption isotherms of the nanospheres obtained with and without urea as well as

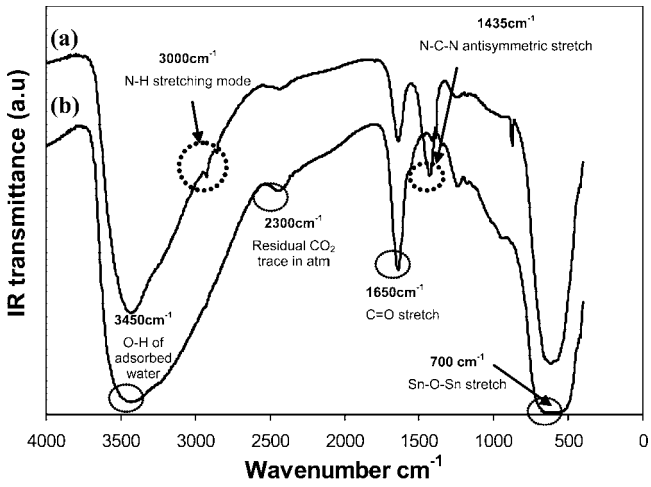

Figure 6. FTIR spectra of samples prepared (a) with and (b) without urea.

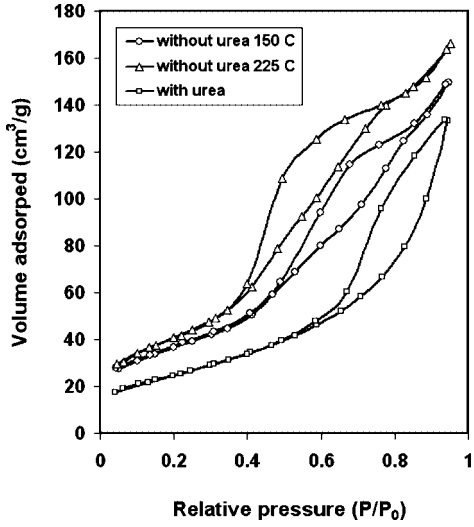

Figure 7. N_2 adsorption−desorption isotherm curves of the samples grown with and without urea as well as different reaction temperatures.

at different growth temperatures. The isotherms curve of samples grown without urea show well-defined steps at a relative pressure (p/p_0) of ~0.4−0.7, which suggests a mesoporous structure of the nanospheres. The samples grown without urea exhibit a higher sorption capability as compared to the sample grown with urea. In addition, use of urea also has a strong influence on the specific surface area of the SnO_2 nanospheres. In comparison, the specific surface area of the sample with urea is relatively lower (101.38 m^2/g), while the sample grown without urea at lower temperature (150 °C) has a higher specific surface area (142.3 m^2/g). The sample grown without urea and at higher temperature (225 °C) exhibits the highest specific surface area of 156.40 m^2/g. The TEM image of Figure 4f shows that there is a greater porosity for the higher temperature due to a greater extent of dissolution. It is also worthwhile to mention that use of urea leads to a significant reduction in the specific surface area of the samples. Oxide surfaces permit easy adsorption of the N_2 gas molecules due to the large number of surface dangling bonds,[22] and it is postulated that the lower specific surface area is due to the presence of urea molecules in the SnO_2 nanospheres which effectively reduces the number of bonds available for N_2 gas adsorption. Thus, this is an added benefit of eliminating urea from our synthesis procedures since nanostructures of high specific surface area and superior surface reactivity are greatly desired for use as catalysts and gas sensors, which will be reported separately.

Conclusion

The porosity of SnO_2 nanospheres can effectively be tuned via a facile and easily scalable hydrothermal process. Longer reaction times and high temperatures were shown to facilitate dissolution of the nanospheres, thus rendering the structures to be more porous in nature. The as-prepared mesoporous structures were formed by self-assembly of numerous single-crystal nanocrystallites of diameter 5−10 nm. The growth mechanism of imperfect oriented attachment is proposed based on electron microscopy analysis. Understanding the growth mechanism and effect of reaction parameters on the chemical and structural components of the SnO_2 mesoporous spheres is important for rational designing of other inorganic mesoporous structures. Most importantly, the employed method requires no physical templates or undesirable additives.

Acknowledgment. This work was supported by the National University of Singapore (NUS), grants R-533000002123 and R533000003112. The authors would like to thank the Surface Science Lab for the use of XPS.

References

(1) Sakai, G.; Nam, S. B.; Miura, N.; Yamazoe, N. *Sen. Actuators B* **2001**, *77*, 116–121.
(2) Hu, J. Q.; Ma, X. L.; Shang, N. G.; Xie, Z. Y.; Wong, N. B.; Lee, C. S.; Lee, S. T. *J. Phys. Chem.* **2002**, *106*, 3823–3826.
(3) Nicholas, C. P.; Marks, T. J. *Nano Lett.* **2004**, *4*, 1557–1559.
(4) Kim, C.; Noh, M.; Choi, M.; Cho, J.; Park, B. *Chem. Mater.* **2005**, *17*, 3297–3301.
(5) Caruso, F. *Chem.−Eur. J.* **2000**, *6*, 413–419.
(6) Wang, C.; Chu, X.; Wu, M. *Sens. Actuators B* **2007**, *120*, 508–513.
(7) Nützenadal, C.; Züttel, A.; Chartouni, D.; Schmid, G.; Schlapbach, L. *Eur. Phys. J. D* **2000**, *8*, 245–250.
(8) Kaciulis, S.; Mattogno, G.; Galdikas, A.; Mironas, A.; Setkus, A. *J. Vac. Sci. Technol. A* **1996**, *14*, 3164–3168.
(9) Caruso, F.; Shi, X.; Caruso, R. A.; Susha, A. *Adv. Mater.* **2001**, *13*, 740–744.
(10) Liu, T.; Xie, Y.; Chu, B. *Langmuir* **2000**, *16*, 9015–9022.
(11) Lou, X. W.; Yuan, C.; Rhoades, E.; Zhang, Q.; Archer, L. A. *Adv. Funct. Mater.* **2006**, *16*, 1679–1684.
(12) Qi, L. M.; Li, J.; Ma, J. M. *Adv. Mater.* **2002**, *14*, 300–303.
(13) Lou, X. W.; Wang, Y.; Yuan, C.; Lee, J. Y.; Archer, L. A. *Adv. Mater.* **2006**, *18*, 2325–2329.
(14) Ahn, H. J.; Choi, H. C.; Park, K. W.; Kim, S. B.; Sung, Y. E. *J. Phys. Chem. B* **2004**, *108*, 9815–9820.
(15) Im, J. S.; Park, S. J.; Lee, Y. S. *J. Colloid Interface Sci.* **2007**, *314*, 32–37.
(16) Penn, R. L.; Banfield, J. F. *Science* **1998**, *281*, 969–971.
(17) Yang, H. G.; Zeng, H. C. *J. Phys. Chem. B* **2004**, *108*, 3492–3495.
(18) Miao, Z.; Wu, Y.; Zhang, X.; Liu, Z.; Han, B.; Ding, K.; An, G. *J. Colloid Interface Sci.* **2007**, *314*, 1791–1796.
(19) Cao, G. *Nanostructures and Nanomaterials: Synthesis, Properties and Applications*; Imperial College Press: London, 2004; Chapter 2, pp 38−42.
(20) Ocana, M.; Serna, C. J.; Matijevi, E. *Colloid Polym. Sci.* **1995**, *273*, 681–686.
(21) Fujihara, S.; Maeda, T.; Ohgi, H.; Imai, J.; Kim, S. *Langmuir* **2004**, *20*, 6476–6481.
(22) Sze, S. M. *Semiconductor Sensors*; Wiley: New York, 1994; Chapter 8, pp 384−389.

CG8001256